Photovoltaic generation on vertical façades in urban context from open satellite-derived solar resource data

Jesús Polo [1*], Nuria Martín-Chivelet[1], Miguel Alonso-Abella[1], Carmen Alonso-García[1]

[1] Photovoltaic Solar Energy Unit (Renewable Energy Division, CIEMAT), Avda. Complutense 40, 28040 Madrid, Spain

* Corresponding author
Jesús Polo, email: jesus.polo@ciemat.es, Phone: +34 914962513, Fax : +34 913466037

Abstract

Solar radiation incident at building façades and elements in an urban context is essential in determining the energy production on building rooftops and vertical façades. The proper determination of solar irradiance incident on a vertical façade needs quality input of the components of solar radiation and a high resolution digital surface model with the heights of buildings and other elements in the urban area of study. In this work a thorough methodology for modeling PV generation, in hourly basis, at building façades with open available data and methods is presented. Hourly data of satellite-derived solar irradiance is used with high resolution digital model from LIDAR information to estimate with the Sandia model the PV generation of five small arrays at west, south and east façades of a building in Madrid. PV output modeled for west and south arrays are in rather good agreement with the monitored experimental data of the production. RMSE of 8% and 12% was observed for the monthly power predicted for west and south facades, respectively. The east façade case was much more challenging due to variability of shadows it receives from the nearby large deciduous trees throughout the year, which results in high uncertainty in the shading influence estimation. Anyway, the methodology proves the benefits and possibilities of detailed estimation of PV production in building façades from open available information regarding both solar resource, open modeling tools and urban topography, even in a very challenging conditions associated to the variability of trees canopy.

Keywords: BIPV; PV modeling; Solar Radiation databases; Sky View Factor; Digital Surface Model; partial shading of PV arrays

1. Introduction

Solar photovoltaics (PV) and solar thermal systems deployments in urban environments are gaining interest as drivers of decentralization of electricity and heat production. Both are key elements in the concept of Nearly Zero-Energy Buildings (nZEB) aimed at achieving buildings almost independent from the external electrical grid through proper designed features and the use of renewable energy sources (Marszal et al., 2011). In the case of PV, the International Energy Agency, through the Task 15 of the programme IEA-PVPS (PVPS, 2021), is gathering efforts in promoting and accelerating the penetration of both BIPV (Building Integrated PhotoVoltaics) and BAPV (Building Applied PhotoVoltaics), and delivering updated reports on important aspects as regulation, definition and characterization, user needs and research. Solar potential studies in urban landscape can include ground, roofs and vertical façades of buildings.

Many studies in the literature dealt with solar potential estimation on rooftops using geographic information systems (GIS) to incorporate the influence of urban obstructions to the incoming solar radiation (Bódis et al., 2019; Brito et al., 2012; Jakubiec and Reinhart, 2013; Khan and Arsalan, 2016; Singh and Banerjee, 2015; Verso et al., 2015). However, in the past recent years additional studies include methodologies for estimating solar potential also in vertical façades (Catita et al., 2014; Desthieux et al., 2018; Hofierka and Zlocha, 2012; Lindberg et al., 2015; Lou et al., 2016; Redweik et al., 2013). A thorough review on modeling the solar potential in urban context can be found in the recent literature (Freitas et al., 2015). Recent studies combine GIS, physics models and machine learning algorithms at national scale (Assouline et al., 2018; Walch et al., 2020). Moreover, recent contributions are conducting also to the availability of open and powerful tools broadening the possibilities of new studies and analysis. For instance this is the case of SEBE (Solar Energy on Building Envelopes) model which is incorporated in UMEP (Urban Multi-scale Environmental Predictor), a plugin for QGIS software (QGIS, 2021). SEBE model estimates solar irradiance on ground surfaces, building roofs and walls from digital surface model (DSM) and solar position (Lindberg et al., 2015; Ratti and Richens, 1999).

The models and tools for estimating solar potential in complex urban environment require also detailed information of solar resource. Solar radiation data on vertical surfaces are not generally available from measurements and the procedure involves having data of the three components of solar irradiance for horizontal surface: Global Horizontal Irradiance (GHI), Direct Normal Irradiance (DNI) and Diffuse Horizontal Irradiance (DIF). Then, the subsequent use of transposition models is needed afterwards to derive the incident solar irradiance at vertical surfaces. The accuracy and quality of the initial solar radiation data plays a significant role on the final uncertainty since there are many intermediate steps in the procedure of estimating solar irradiance incident on façades. Satellite-derived solar irradiance data is probably the best choice nowadays since there are several high quality products that are freely available(Polo and Perez, 2019; Sengupta et al., 2017). Time series of GHI, DNI and DIF can be obtained on an hourly basis from several databases with rather good quality (de Freitas Moscardini Júnior and Rüther, 2020; Huld et al., 2012; Polo et al., 2020; Psiloglou et al., 2020; Riihelä et al., 2015; Urraca et al., 2017; Yang, 2018; Yang and Bright, 2020). Afterwards, transposition models are then needed to estimating solar irradiance at an inclined and arbitrarily oriented surface using the three components (GHI, DNI, DIF) as input. There is a very large list of transposition models elsewhere and recent studies contain useful information on their accuracy and associated difficulties and problems (Gueymard and Ruiz-Arias, 2016; Yang, 2016).

This work presents a thorough methodology for modeling in detail the PV generation of five small PV arrays placed at the vertical façades of a building in Madrid using as input open satellite-derived solar radiation data and LIDAR information. A DSM is built from the LIDAR data to estimate shading and the corresponding sky view factor (SVF). Two years of hourly solar radiation is used as input to derive solar irradiance in high detail for the façades of the building. Most works in the literature employ GIS for studying the potential mainly on rooftops and less frequently in facades in terms of yearly values or annual yield, but very few studies presents estimations at hourly basis and assessment with real monitored PV arrays working on facades of a building. The results show the benefit of the methodology for modeling the PV generation of modules at façades and also evidence the potential problems associated to the presence of large trees near the façade that may affect to the proper shading effect determination; particularly interesting is the case of deciduous trees, which opacity changes throughout the year.

2. Description of the case study and experimental data

The building under study is the so-called *Building 42* of Ciemat headquarters area, placed in the university campus in Madrid (40.4551° North, -3.73° East). This building houses five individual small PV arrays (each one connected to a different single inverter) distributed in the upper part of the east, south and west façades. The orientation of the building is slightly deviated to the west (about 9°) and thus the façades azimuth are 351°, 81°, 171° and 262° for façades north, east, south and west, respectively. Figure 1 shows the domain area used in this work and pictures of the PV arrays in façades east, south and west. The east façade contains three identical PV arrays of 7sx2p modules (named East_S, East_C and East_N arrays, respectively), the south façade has one array of 7sx4p modules, and the west façade includes one 8sx2p PV array. Table 1 summarizes the module and inverter characteristics of all the arrays. Additional details on the building structures, PV systems and monitoring can be found in a previous descriptive work (Martín-Chivelet et al., 2018).

Figure 1. a) Area of study of Ciemat headquarters. b) East façade with three PV arrays highlighted. c) South façade with the corresponding PV array. d) West façade with the PV array used in this work.

Table 1. Main characteristics of the PV arrays

Array	Configuration	Module	Power (W)	Inverter	Power (kW)
East_N	7sx2p	SunPower E20-327	327	Fronius IG Plus 50 V-1	4
East_C	7sx2p	SunPower E20-327	327	Fronius IG Plus 50 V-1	4
East_S	7sx2p	SunPower E20-327	327	Fronius IG Plus 50 V-1	4
South	7sx4p	SunPower E18-325	305	Fronius IG Plus 100 V-3	8
West	8sx2p	SunPower E20-327	327	Fronius IG Plus 50 V-1	4

Different electrical parameters of each array as well as some local meteorological variables are being monitored. In particular, voltage, current and power of each inverter are available. In addition, module temperature of one single module from each array is measured using T type thermocouples. Global horizontal irradiance (GHI) is measured in the rooftop of the building with a thermopile pyranometer and vertical irradiance in east, south and west orientations of the building are also recorded by several calibrated cells placed at the top of a mast in the building rooftop (Figure 2). Unfortunately there were not available long and quality measurements of direct normal irradiance (DNI) and diffuse horizontal irradiance (DHI). Figure 2 shows also how the modules were integrated and fastened to the façade in the upgrading work of the building. PV modules are integrated into the upper areas of a new ventilated façade, built as part of the rehabilitation project for Ciemat building 42, which was aimed at improving the building's structural condition and energy efficiency. PV modules occupy a total surface area of about 176 m2.

a) **b)**

Figure 2. a) Mast placed at the building rooftop with calibrated cells for measuring vertical irradiance at east, south and west orientations. b) Solar panels integration with the façade.

3. Solar resource data

The basic solar resource data used as input in this work consisted of two years (2017 and 2018) of hourly data of the three solar irradiance components (GHI, DNI and DIF) delivered by CAMS (Copernicus Atmosphere Monitoring Service) Radiation Service with a spatial resolution of 3 km at nadir (Schroedter-Homscheidt et al., 2019). CAMS Radiation Service (Copernicus, 2021) is a high quality database of solar irradiance based on Heliosat-4 methodology (Qu et al., 2017). The method combined the cloud properties derived from Meteosat Second Generation (MSG) satellites with fast radiative transfer model McClear (Lefèvre et al., 2013). CAMS GHI hourly data compared with the GHI measurements on the building rooftop resulted in mean bias deviation (MBD) of -0.5 % and root mean square deviation (RMSD) of 17.4 %. Figure 3 shows a scatter plot for the assessment of GHI delivered by CAMS Radiation Service for the period 2017-2018; the corresponding R^2 for this scatter plot is 0.95. Despite there is no quality measurements of DNI for evaluating the uncertainty of DNI derived by CAMS Radiation Service it is expected to be higher than the uncertainty for GHI. For instance, evaluation of CAMS radiation service in several ground stations in Morocco resulted in RMSD for hourly DNI in the range of 26-39% (Marchand et al., 2018). Nevertheless, it should be remarked that CAMS Radiation Service is one of the best and more accurate free and open products for solar radiation data derived from satellite imagery (Yang and Bright, 2020).

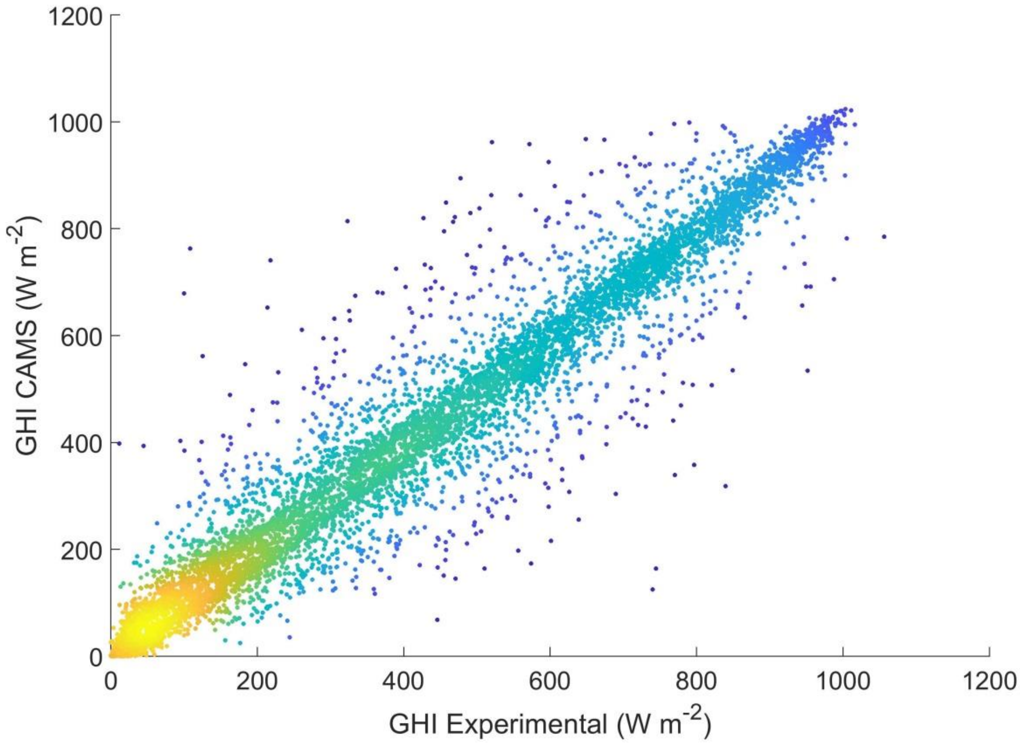

Figure 3. Scatter plot of hourly GHI estimated by CAMS vs. experimental measurements in Building 42.

4. Solar irradiance at vertical façades

4.1 Sky view factor and Shadow calculation

The sky view factor (SVF) is a simple parameter describing the part of the sky that is not obscured by the surroundings for a given point (Lindberg and Grimmond, 2010). It can be defined as the ratio of the sky hemisphere visible from the ground (Bernard, 2018). The SVF and the shadowing in the façades of a building can be computed from a high-resolution digital surface model (DSM) derived from LIDAR data. LIDAR data offers the height of a ground area with very high resolution (including buildings, trees, structures, etc). In Spain LIDAR data is supplied by the Spanish Geographic Institute (IGN) through a download service (Centro Nacional de Información Geográfica, 2021).

In this work a DSM of the area under study is obtained with the use of LASTools (a powerful library for reading and extracting information from compressed LIDAR files) and QGIS. The resulting raster DSM of the area of Ciemat including the *Building 42* and surrounding buildings, elements and trees is shown in figure 4. The DSM shown in this figure covers the same area of that shown in Figure 1 a), so that the identification of the building under study in figures 4 a) and b) is straightforward. It should be remarked that north and east façades of the building have many large trees placed close to the building, while south and west-south façades have mainly other buildings in the surroundings.

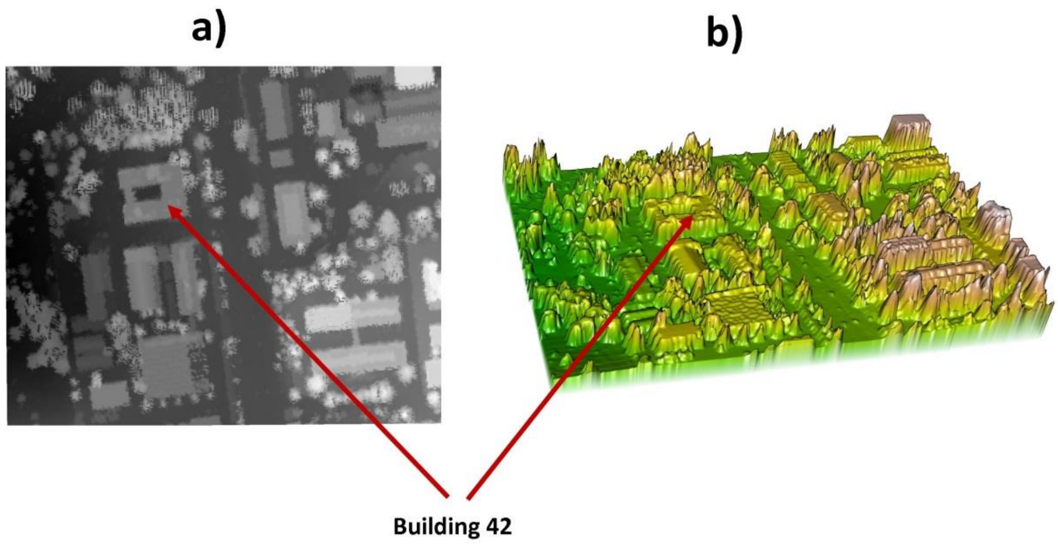

Figure 4. a) Geotiff raster of DSM. b) 3-D view of DSM.

Four artificial façades for the target building have been created by selecting the corresponding x-utm and y-utm coordinates of the points delimiting each building façade in the DSM with a resolution of around 25 cm in length and 0.5 m in height. The total height of each artificial façade is 15 m, so that it is higher than the actual façades heights of 8 and 10 m, depending on the façade. Thus a façade is a matrix of 31 rows (denoting points at different heights) by 150-175 columns (defined by x-utm and y-utm coordinates of the real façades).

For each point (i, j) in the façade matrix, the SVF for the façade *F* is computed by the following expression (Böhner and Antonić, 2009):

$$SVF^F(i,j) = \frac{1}{N} \sum_{n=1}^{N} [cos\beta \ cos^2 \emptyset_n(i,j) + \ \sin\beta \cos(n - \alpha_F)(90 - \emptyset_n(i,j) - sin\emptyset_n(i,j) cos\emptyset_n(i,j) \ ) \ ]. \quad (1)$$

Where N is 360°, β is the tilt angle of the surface (90° for a vertical façade), n is a direction in azimuth (it ranges from 1 to 360 in steps of 1°), α_F is the azimuth of the façade *F*, and $\emptyset_n(i,j)$ is the horizon angle of point (i,j) in the azimuth direction determined by n. The horizon angle $\emptyset_n(i,j)$ is determined by the angle of elevation of the highest obstacle (point in the DSM) that the point (i,j) views in the azimuth determined by n.

Figure 5 shows the SVF computed for the four façades of *Building 42* taking into account the obstacles in the area delimited by the DSM. It can be clearly appreciated the strong influence of the large trees on the North-East corner of the building.

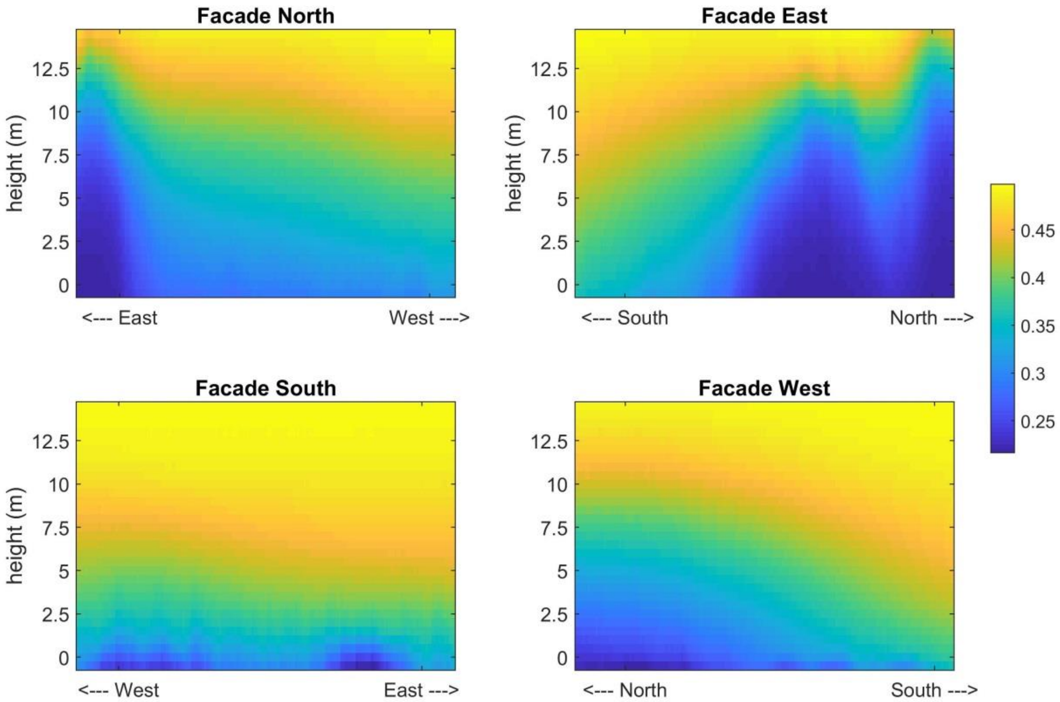

Figure 5. SVF computed for the four façades of CIEMAT Building 42.

Shadows are computed in hourly basis for each element of the façade (25 cm wide and 50 cm in height) as a parameter, that can only takes two values, *Sh*=1 if the element is illuminated and *Sh*=0 if the element is shadowed. Thus, for every façade we have a matrix of shadow for every hour indicating which elements in the façade are completely shadowed and which ones are completely illuminated every hour.

4.2 Solar irradiance at vertical façades

In order to estimate the incident hourly solar irradiance at each point of the façade F we have assumed the following approach,

$$G^F(i,j) = DNI \cos(AOI)\, Sh(i,j) \;+\; Diff^F(i,j) \;+\; \tfrac{1}{2}\rho^F \, GHI \;, \qquad (2)$$

where AOI is the angle of incidence which depends on the solar elevation and azimuth angles and on the surface's tilt (90° for every façade) and azimuth angles, $Diff^F(i,j)$ is the sky diffuse irradiance for the element (i,j) of façade *F*, and ρ^F is the effective albedo for façade *F*, defined here as the average albedo of the ground and surrounding surfaces that can reflect solar irradiance towards the façade (the values of 0.2 has been chosen for the effective albedo). Therefore, the incident solar irradiance on the façade element is the sum of three contributions, the direct irradiance projected to the surface taking into account the shading, the sky diffuse irradiance and the reflected irradiance due to ground and other surfaces and elements in the surrounding. The Diffuse irradiance is computed from the three components of horizontal irradiance by the Perez model with modifications to take into account the sky view factor of each element in the façade (Perez et al., 1990, 1987). The sky diffuse irradiance is then estimated by,

$$Diff^F(i,j) = Cir^F Sh(i,j) \;+\; DIF\; SVF^F(i,j) + Hor^F \;, \qquad (3)$$

being Cir^F and Hor^F are the circumsolar diffuse component and horizon brightening diffuse component of the solar radiation estimated by Perez model, respectively. Therefore, the main modification to the original Perez model for tilt surface consisted on taking into account the shading in the circumsolar diffuse component and the sky view factor of every façade element in the isotropic diffuse irradiance instead of the sky view factor determined only by the tilt angle (0.5 for the case of a vertical surface). Therefore, using the GHI, DNI and DIF satellite-derived components provided by CAMS Radiation Service as input and the sky view factor and shading estimated from the DSM is suitable to estimate the incident solar irradiance at each façade element.

4.3 Evaluation of solar radiation estimations at façades

In order to evaluate the uncertainty of the solar irradiance estimations made on the building façades we have compared them with the measurements of the calibrated solar cells placed at the top of a mast on the building rooftop (Figure 2). The corresponding MBE, RMSD and MAD (Mean Absolute Deviation) are shown in table 2. Figure 6 shows the east, south and west solar irradiance estimated compared with measurements in hourly basis for a few days and the corresponding scatter plots. The R^2 estimated for these scatter plots were 0.73, 0.89 and 0.90 for the east, south and west facades, respectively.

Table 2. Error metrics for solar irradiance estimated at vertical façades

Façade	MBD (%)	RMSD (%)	MAD (%)
East	5.7	57.3	32.0
South	5.6	29.8	18.4
West	-6.2	32.1	18.8

As shown in both the table and the scatter plots of figure 6 much higher uncertainty resulted in the estimations of solar irradiance at the east façade. As a consequence much higher uncertainties are also expected in modeling those PV arrays placed on east façade.

The scatter plot for east façade shows a set of data that are particularly underestimated (Figure 6). This underestimation is due to the uncertainty associated to the large deciduous trees in front of the east façade of the building. On the one hand, DSM information that comes from LIDAR data might not include recent possible changes in the natural vegetal cover (i.e. tree pruning), or refurbishment works after LIDAR flights; on the other, during fall and winter seasons the deciduous trees opacity is much less than in spring and summer, and consequently direct radiation can reach the wall of the building while the modeling calculates a shadowing. Therefore, the line of deciduous trees close to the east facade, taller than the building height, is very challenging for modeling both the solar irradiance and the PV generation at the façade.

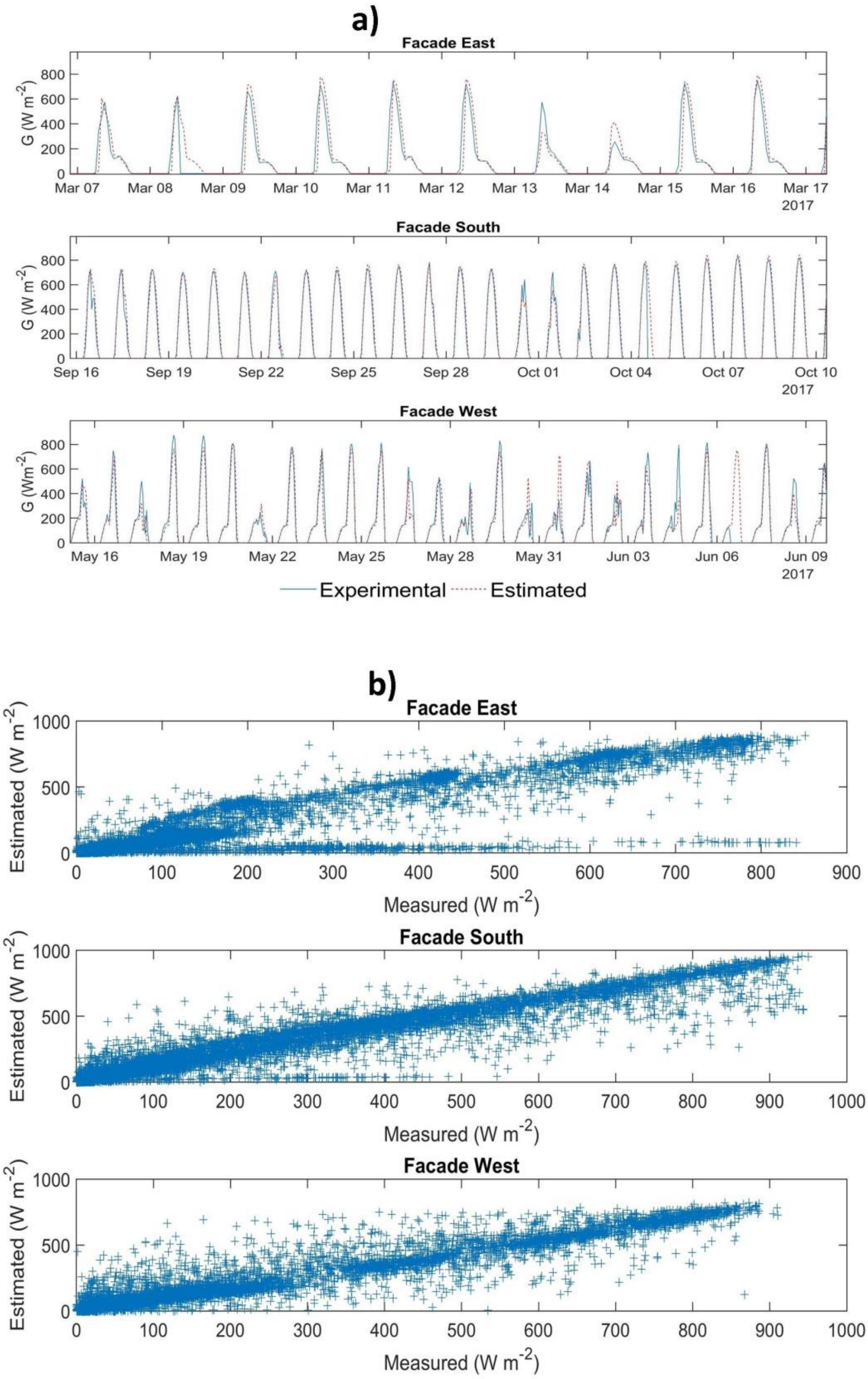

Figure 6. Solar irradiance estimated for the vertical façades compared with experimental data. a) Example of several days. b) scatter plot of hourly data.

5. Modeling the PV generation at the three façades

The energy generation of the five PV arrays listed in table 1 has been modeled for two years (2017 and 2018) with the Sandia Array Performance Model (SAPM) using as input the solar irradiance, in hourly basis, estimated at the façade points, with a resolution of 50x25 cm, and the module temperature measured at each array. Back panel temperature was measured with one thermocouple for every array at the rear side of the modules, and was directly input to the SAPM model. SAPM is available under the PV Performance Modeling Collaborative initiative (King et al., 2007, 2004). SAPM model is included in the PV lib library that can be freely downloaded from the PVPCM site (PVPCM, 2021) and has shown to be very flexible and accurate (Gurupira and Rix, 2017; Polo et al., 2016; Stein and Farnung, 2017).

Since the irradiance incident at each array varies along the surface due to shading, the DC part of the PV generation has been modeled individually for every single module in the array and then the array configuration has been taken into account for estimating the DC generation of the whole array. Thus, SAPM model is used to model the DC power of every single module in the array using as input the average incoming solar irradiance over the module area and the module temperature measured (we have only one measuring point for the module temperature for each array). Modeling partial shading in PV arrays is complex and can involve to deal module by module, or cell by cell, with the whole I-V curve (Alonso-García et al., 2006; Alqaisi and Mahmoud, 2019; Galeano et al., 2018; Seyedmahmoudian et al., 2013). Shading losses depend on the series-parallel configuration of the array, the number and distribution of by-pass and blocking diodes and on the shading profile (Alonso-García et al., 1997). Due to the complexity of the problem and the uncertainties in determining accurately the shading and the limitations of the SAPM model it was required the adoption of approximations to explore the capabilities of simple and fast models in modeling these arrays at the different façades.

Two different approaches have been explored to model the array power generation under complex and irregular shading effects. The first one, denoted as Model 1, assumes that each string in the array is working with the maximum current as it would not be affected by shading, and the AC power is finally multiplied by the fraction of the area that is shaded to account for the reduction of power due to shading. The approach of assuming that the power reduction is equal to the shaded array fraction is the most optimistic and represent the minimum limit for power reduction (Martínez-Moreno et al., 2010; Masa-Bote and Caamaño-Martín, 2014). The second approach, denoted as Model 2, assumes that the string working current is limited by the shaded modules and then the minimum current of module is assumed for the whole string, and consequently the AC power of the array is not multiplied by any shading factor at all.

Figure 7 shows the daily generation of each array during for the two years modeled. Arrays at west and south façades are generally better modeled than those at east façade. The power output in west and south arrays was predicted with a RMSE of 15% and 21%, respectively, in daily basis, and in monthly basis the RMSE was 8% and 12%, respectively. In addition, it can be observed that the uncertainty in estimating the daily production varies along the length of the east façade. The highest differences between experimental and modeled energy production are found in the north part of the east façade (the so called East_N array). Figure 8 shows the box plot of the differences between hourly experimental power and hourly modeled power with model 2 for each array.

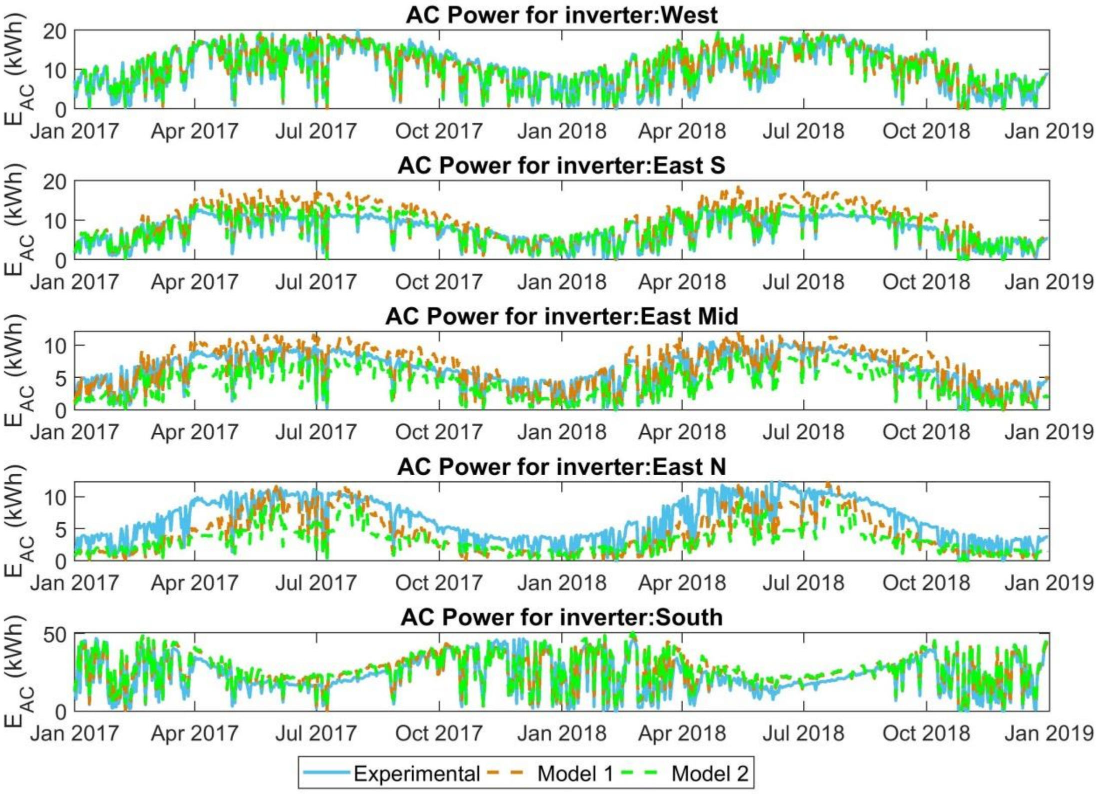

Figure 7. Daily energy production of PV arrays at façades compared to the monitored data.

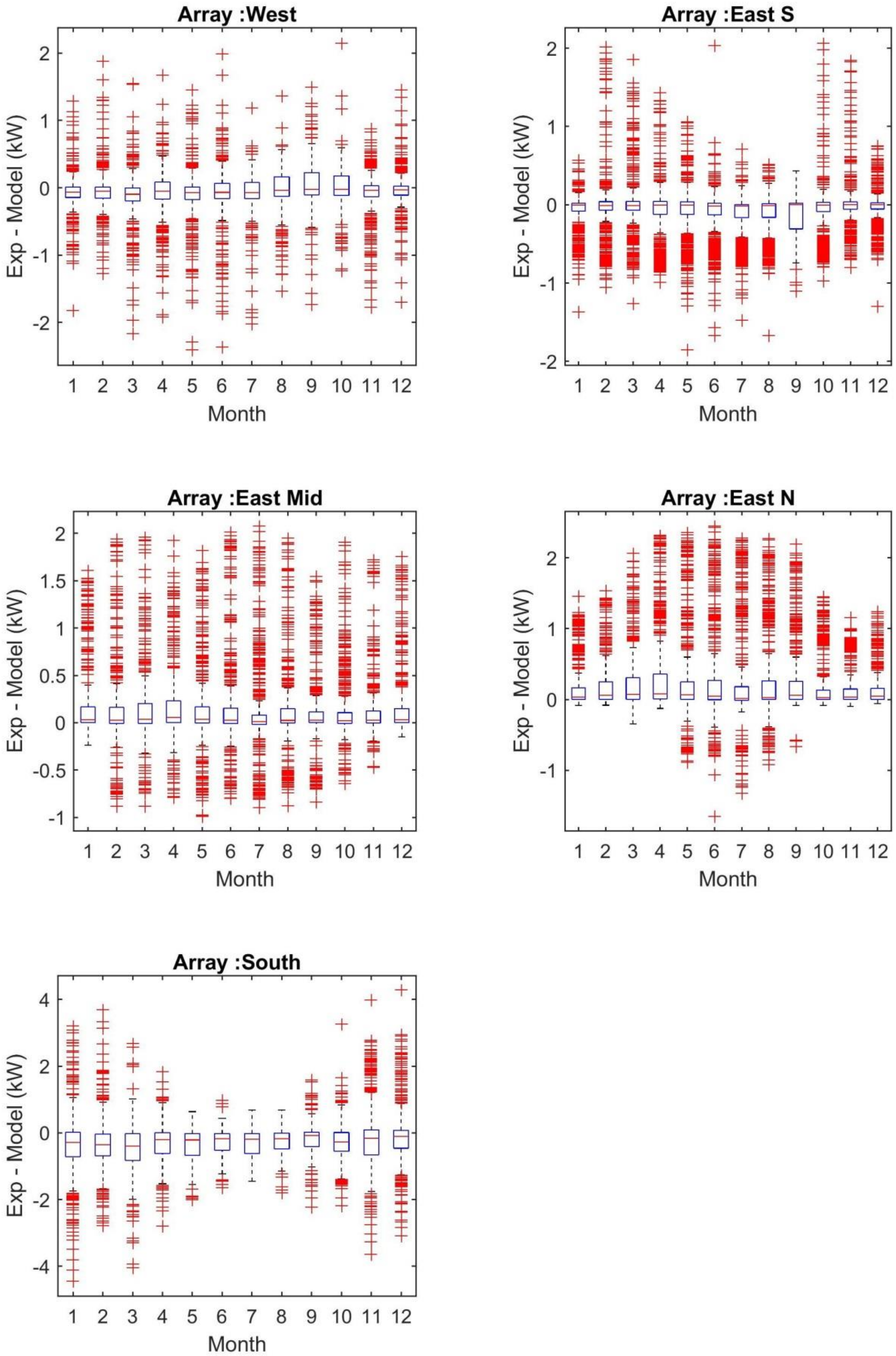

Figure 8. Box plot of differences between experimental and modeled power in hourly basis.

In the case of the three arrays placed at the east façade the modeling results with the Model 1 show a general overestimation of the energy throughout the whole year, excepting the case of array East_N (placed at the north part of the façade), where the trend is a general and significant underestimation. However, the results of the Model 2 show higher agreement with the experimental data in arrays East_S and East_Mid, but larger underestimations of the output power in array East_N during spring and summer. The Model 2 approach has more physical meaning since the shaded modules limit the final current in the string they form part of, and thus a better performance was expected. However, the large uncertainties in these arrays at the east façade evidence the uncertainties in the shading determination due to irregular and changing shading conditions produced by the surrounding trees.

Therefore, this apparently opposite behavior in the predictions of arrays placed at the same façade can be only explained by the different shading modeled along the year, its dynamics and variability, and the impact on the challenging conditions imposed to the array. Thus, the irregular and dynamic conditions of the shading caused by the deciduous trees in front of the east façade make it quite difficult to model accurately the arrays generation by using simple performance models as SAPM. In addition to the propagation of the initial uncertainty of solar radiation components derived from a satellite model, one even most important contributor to the uncertainty is the impact of the limitations in the DSM obtained from LIDAR information. Thus, the information in the digital model corresponds to a steady picture of the heights of surrounding objects. Figure 9 shows a picture of the whole east façade in a summer morning where irregular characteristics of the shading can be clearly observed. As can be seen in the picture in front of the east-north façade there is a dry tree without leaves that would explain the underestimation of the energy generated by the array East_N. Thus, according to the DSM there is a large tree there, which implies a tall obstacle to the incoming solar irradiance while the actual situation is different. That tree is actually rather transparent to the incoming solar irradiance and the underestimation observed in the calculation is due to erroneous computation of the shading in that part of the building. In addition, in the DSM it can be observed two additional trees at the north-east corner of the building that no longer exist (see and compare figure 4 and the picture in figure 9). Indeed, the trees shown in the east-north corner of the building were removed before the installation of the PV modules in the building façades, indicating that the LIDAR information available for the area of study is not updated to the show the refurbishment works performed in the building in 2016. In addition, figure 10 illustrates the shadow induced by the trees, modeled from the DSM data, for three different hours in a single day, where it can be appreciated the irregular shapes of the shadows.

Figure 9. Irregular shading on the east facade caused by trees in a summer morning.

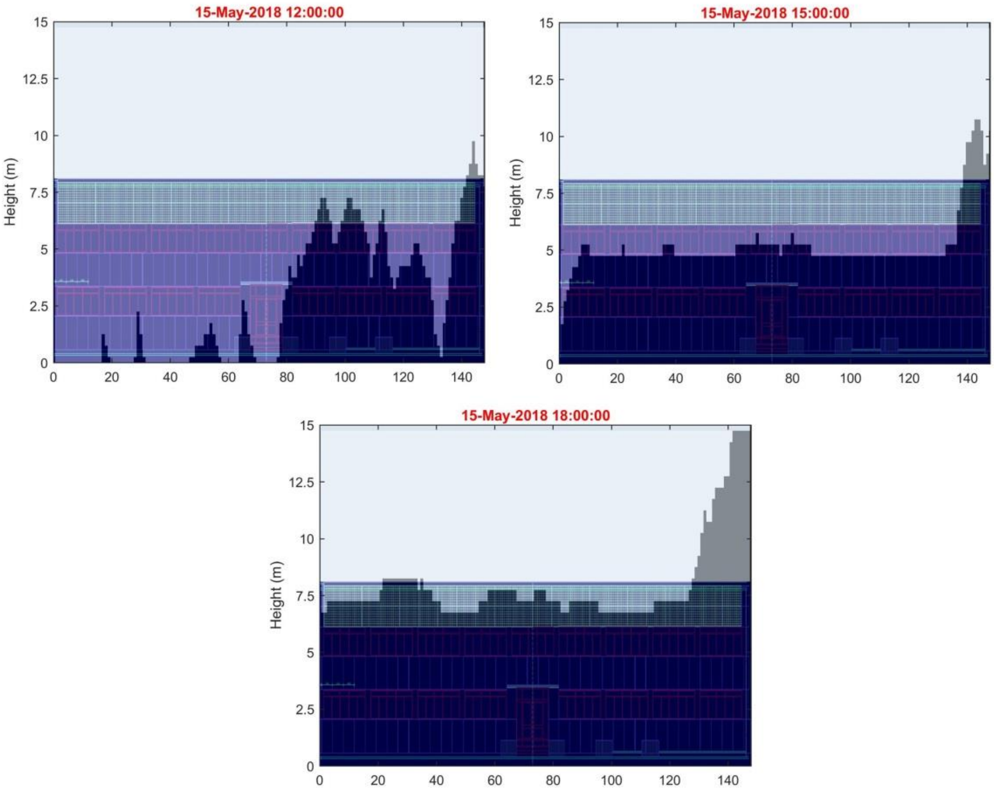

Figure 10. Computed shadows on east façade for three different hours (12:00, 15:00 and 18:00) on a 15th may 2018.

5. Conclusions

Detailed modeling of PV generation at the façades of a building in urban environment requires of both time series of solar irradiance components with good quality and high resolution information on the morphology of the environment to allow shadow casting estimates. There are several open databases of solar radiation data derived from satellite imagery that can be effectively used for that purpose. In addition, the urban morphology can be obtained from LIDAR data to create DSM at high resolution with the heights of buildings, canopies, trees and other structures. This work presents a methodology for modeling PV generation on building façades based entirely on open and free data and methods available. Solar resource basic input consisted of time series of the solar radiation components, in hourly basis, supplied by CAMS Radiation Service for two years (2017 and 2018). Open GIS tools and LIDAR data have been used to create a DSM of a selected area in the university campus of Madrid. Shading and sky view factor have been then computed, from the DSM, for the façades of a selected building in the area of study, where five small PV arrays are installed in façades west, south and east, and monitored. Thus, detailed estimations of incident solar irradiance at each point of every façade are performed by combining shading and SVF parameters with Perez transposition model. Finally, modeling of PV generation of each array was performed by using the SAPM model implemented in PV lib open tool. The methodology presented here thus is aimed at proving that by using free public data and models it is possible to perform a thorough analysis of the PV generation at a building façade in Madrid City. Notwithstanding the study did not need a priori of satellite derived irradiance, since we has measurements of incident irradiance at three directions, the use of open satellite data allows to remark the potentiality of the methodology for future extension at large scale.

The results of PV modeling at façades shown in this work have proven the benefit of this methodology for façades in buildings. The west and south arrays were modeled with good results. However, challenging boundary conditions regarding large deciduous trees close to the east façade have evidenced large uncertainties and difficulties in proper modeling the PV arrays due to the changes throughout the year of trees opacity. On the other hand, recent changes of removing some trees are not contemplated in the DSM since LIDAR data provides information before 2016 (year of refurbishment of the building and surroundings). In other words the static feature of the DSM limits somehow its use in modeling those facades that might be affected by dynamic changes in the surrounding tress and vegetation. The impact of this dynamic partial shading on the arrays at east façade requires a more detailed analysis and the use of complex models that account better for partial shading effects. Future work motivated from these results will be focused on better modeling the performance of these arrays at east façade under the challenging conditions imposed by the presence of large trees in the surroundings.

Acknowledgements

The authors would like to recognize the efforts, research and contributions of the experts groups of IEA PVPS programs, in particular those corresponding to task 15 (BIPV) and task 16 (Solar Resource), where the authors collaborate.

References

Alonso-García, M.C., Arribas, L.M., Chenlo, F., Cruz, I., 1997. Shading Effect on a Roof Integrated Grid-Connected PV Plant, in: 14th European Photovoltaic Solar Energy Conference, EUPVSEC. Barcelona, Spain.

Alonso-García, M.C., Ruiz, J.M., Herrmann, W., 2006. Computer simulation of shading effects in photovoltaic arrays. Renewable Energy 31, 1986–1993. doi:10.1016/j.renene.2005.09.030

Alqaisi, Z., Mahmoud, Y., 2019. Comprehensive Study of Partially Shaded PV Modules with Overlapping Diodes. IEEE Access 7, 172665–172675. doi:10.1109/ACCESS.2019.2956916

Assouline, D., Mohajeri, N., Scartezzini, J.L., 2018. Large-scale rooftop solar photovoltaic technical potential estimation using Random Forests. Applied Energy 217, 189–211. doi:10.1016/j.apenergy.2018.02.118

Bernard, J., 2018. Sky View Factor Calculation in Urban Context : Computational Performance and Accuracy Analysis of Two Open and Free GIS Tools. climate 6. doi:10.3390/cli6030060

Bódis, K., Kougias, I., Jäger-Waldau, A., Taylor, N., Szabó, S., 2019. A high-resolution geospatial assessment of the rooftop solar photovoltaic potential in the European Union. Renewable and Sustainable Energy Reviews 114, 109309. doi:10.1016/j.rser.2019.109309

Böhner, J., Antonić, O., 2009. Land-surface parameters specific to topo-climatology. Developments in Soil Science 33, 195–226. doi:10.1016/S0166-2481(08)00008-1

Brito, M.C., Gomes, N., Santos, T., Tenedório, J.A., 2012. Photovoltaic potential in a Lisbon suburb using LiDAR data. Solar Energy 86, 283–288. doi:10.1016/j.solener.2011.09.031

Catita, C., Redweik, P., Pereira, J., Brito, M.C., 2014. Extending solar potential analysis in buildings to vertical facades. Computers & Geosciences 66, 1–12. doi:10.1016/j.cageo.2014.01.002

Centro Nacional de Información Geográfica, 2021. Centro de Descargas [WWW Document]. URL http://centrodedescargas.cnig.es/CentroDescargas/ (accessed 6.8.21).

Copernicus, 2021. CAMS Radiation Service [WWW Document]. URL http://www.soda-pro.com/es/web-services/radiation/cams-radiation-service (accessed 6.8.21).

de Freitas Moscardini Júnior, E., Rüther, R., 2020. The influence of the solar radiation database and the photovoltaic simulator on the sizing and economics of photovoltaic-diesel generators. Energy Conversion and Management 210, 112737. doi:10.1016/j.enconman.2020.112737

Desthieux, G., Carneiro, C., Camponovo, R., Ineichen, P., Morello, E., Boulmier, A., Abdennadher, N., Dervey, S., Ellert, C., 2018. Solar energy potential assessment on rooftops and facades in large built environments based on lidar data, image processing, and cloud computing. Methodological background, application, and validation in geneva (solar cadaster). Frontiers in Built Environment 4. doi:10.3389/fbuil.2018.00014

Freitas, S., Catita, C., Redweik, P., Brito, M.C.C., 2015. Modelling solar potential in the urban environment: State-of-the-art review. Renewable and Sustainable Energy Reviews 41, 915–931. doi:10.1016/j.rser.2014.08.060

Galeano, A.G., Bressan, M., Vargas, F.J., Alonso, C., 2018. Shading ratio impact on photovoltaic

modules and correlation with shading patterns. Energies 11, 1–26. doi:10.3390/en11040852
Gueymard, C.A., Ruiz-Arias, J.A., 2016. Extensive worldwide validation and climate sensitivity analysis of direct irradiance predictions from 1-min global irradiance. Solar Energy. doi:10.1016/j.solener.2015.10.010
Gurupira, T., Rix, A.J., 2017. PV Simulation Software Comparisons : Pvsyst , Nrel Sam and Pvlib, in: SAUPEC 2017.
Hofierka, J., Zlocha, M., 2012. A New 3-D Solar Radiation Model for 3-D City Models. Transactions in GIS 16, 681–690. doi:10.1111/j.1467-9671.2012.01337.x
Huld, T., Müller, R., Gambardella, A., 2012. A new solar radiation database for estimating PV performance in Europe and Africa. doi:10.1016/j.solener.2012.03.006
Jakubiec, J.A., Reinhart, C.F., 2013. A method for predicting city-wide electricity gains from photovoltaic panels based on LiDAR and GIS data combined with hourly Daysim simulations. Solar Energy 93, 127–143. doi:10.1016/j.solener.2013.03.022
Khan, J., Arsalan, M.H., 2016. Estimation of rooftop solar photovoltaic potential using geo-spatial techniques: A perspective from planned neighborhood of Karachi - Pakistan. Renewable Energy 90, 188–203. doi:10.1016/j.renene.2015.12.058
King, D.L., Boyson, W.E., Kratochvill, J.A., 2004. Photovoltaic Array Performance Model. Sandia Report. doi:10.2172/919131
King, D.L., Gonzalez, S., Galbraith, G.M., Boyson, W.E., 2007. Performance Model for Grid-Connected Photovoltaic Inverters, SAND2007-5036. Contract 38, 655–660.
Lefèvre, M., Oumbe, A., Blanc, P., Espinar, B., Gschwind, B., Qu, Z., Wald, L., Schroedter-Homscheidt, M., Hoyer-Klick, C., Arola, A., Benedetti, A., Kaiser, J.W., Morcrette, J.-J., 2013. McClear: a new model estimating downwelling solar radiation at ground level in clear-sky conditions. Atmos. Meas. Tech 6, 2403–2418. doi:10.5194/amt-6-2403-2013
Lindberg, F., Grimmond, C.S.B., 2010. Continuous sky view factor maps from high resolution urban digital elevation models. Climate Research 42, 177–183. doi:10.3354/cr00882
Lindberg, F., Jonsson, P., Honjo, T., Wästberg, D., 2015. Solar energy on building envelopes – 3D modelling in a 2D environment. Solar Energy 115, 369–378. doi:10.1016/j.solener.2015.03.001
Lou, S., Li, D.H.W., Lam, J.C., Lee, E.W.M., 2016. Estimation of obstructed vertical solar irradiation under the 15 CIE Standard Skies. Building and Environment 103, 123–133. doi:10.1016/j.buildenv.2016.04.005
Marchand, M., Ghennioui, A., Wey, E., Wald, L., 2018. Comparison of several satellite-derived databases of surface solar radiation against ground measurement in Morocco. Adv. Sci. Res 15, 21–29. doi:10.5194/asr-15-21-2018
Marszal, A.J., Heiselberg, P., Bourrelle, J.S., Musall, E., Voss, K., Sartori, I., Napolitano, A., 2011. Zero Energy Building - A review of definitions and calculation methodologies. Energy and Buildings 43, 971–979. doi:10.1016/j.enbuild.2010.12.022
Martín-Chivelet, N., Gutiérrez, J.C., Alonso-Abella, M., Chenlo, F., Cuenca, J., 2018. Building retrofit with photovoltaics: Construction and performance of a BIPV ventilated façade. Energies 11. doi:10.3390/en11071719
Martínez-Moreno, F., Muñoz, J., Lorenzo, E., 2010. Experimental model to estimate shading losses on PV arrays. Solar Energy Materials and Solar Cells 94, 2298–2303. doi:10.1016/j.solmat.2010.07.029
Masa-Bote, D., Caamaño-Martín, E., 2014. Methodology for estimating building integrated photovoltaics electricity production under shadowing conditions and case study. Renewable and Sustainable Energy Reviews 31, 492–500. doi:10.1016/j.rser.2013.12.019
Perez, R., Ineichen, P., Seals, R., Michalsky, J., Stewart, R., 1990. Modeling daylight availability and irradiance components from direct and global irradiance. Solar Energy 44, 271–289. doi:10.1016/0038-092X(90)90055-H
Perez, R., Seals, R., Ineichen, P., Stewart, R., Menicucci, D., 1987. A new simplified version of

the perez diffuse irradiance model for tilted surfaces. Solar Energy 39, 221–231. doi:10.1016/S0038-092X(87)80031-2

Polo, J., Alonso-García, M.C., Silva, J.P., Alonso-Abella, M., 2016. Modelling the performance of rooftop photovoltaic systems under urban Mediterranean outdoor conditions. Journal of Renewable and Sustainable Energy 8, 013502. doi:10.1063/1.4942856

Polo, J., Fernández-Peruchena, C., Salamalikis, V., Mazorra-Aguiar, L., Turpin, M., Martín-Pomares, L., Kazantzidis, A., Blanc, P., Remund, J., 2020. Benchmarking on improvement and site-adaptation techniques for modeled solar radiation datasets. Solar Energy 201, 469–479. doi:10.1016/j.solener.2020.03.040

Polo, J., Perez, R., 2019. Solar radiation modeling from satellite imagery, in: Polo, J.; Martín-Pomares, L., Sanfilippo, A. (Ed.), Solar Resource Mapping - Fundamentals and Applications; Green Energy and Technology. Springer, pp. 183–197. doi:10.1007/978-3-319-97484-2_6

Psiloglou, B.E., Kambezidis, H.D., Kaskaoutis, D.G., Karagiannis, D., Polo, J.M., 2020. Comparison between MRM simulations, CAMS and PVGIS databases with measured solar radiation components at the Methoni station, Greece. Renewable Energy 146, 1372–1391. doi:10.1016/J.RENENE.2019.07.064

PVPCM, 2021. PV LIB [WWW Document]. URL https://pvpmc.sandia.gov/applications/pv_lib-toolbox/ (accessed 6.8.21).

PVPS, I., 2021. Enabling Framework for the Development of BIPV [WWW Document]. Web page. URL https://iea-pvps.org/research-tasks/enabling-framework-for-the-development-of-bipv/ (accessed 6.8.21).

QGIS, 2021. A Free and Open Source Geographic Information System [WWW Document]. URL https://www.qgis.org/en/site/ (accessed 6.8.21).

Qu, Z., Gschwind, B., Lefevre, M., Wald, L., Oumbe, A., Blanc, P., Espinar, B., Gesell, G., Gschwind, B., Klüser, L., Lefèvre, M., Saboret, L., Schroedter-Homscheidt, M., Wald, L., 2017. Fast radiative transfer parameterisation for assessing the surface solar irradiance: The Heliosat-4 method. Meteorologische Zeitschrift 26, 33–57. doi:10.1127/metz/2016/0781

Ratti, C., Richens, P., 1999. Urban Texture Analysis with Image Processing Techniques, in: CAAD Futures99. Atlanta.

Redweik, P., Catita, C., Brito, M., 2013. Solar energy potential on roofs and facades in an urban landscape. Solar Energy 97, 332–341. doi:10.1016/J.SOLENER.2013.08.036

Riihelä, A., Carlund, T., Trentmann, J., Müller, R., Lindfors, A., 2015. Validation of CM SAF Surface Solar Radiation Datasets over Finland and Sweden. Remote Sensing 7, 6663–6682. doi:10.3390/rs70606663

Schroedter-Homscheidt, M., Hoyer-Klick, C., Killius, N., Betcke, J., Lefèvre, M., Wald, L., Wey, E., Saboret, L., 2019. User ’ s Guide to the CAMS Radiation Service (CRS) Status December 2019. ECMWF Copernicus Report.

Sengupta, M., Habte, A., Gueymard, C., Wilbert, S., Renné, D., 2017. Best Practices Handbook for the Collection and Use of Solar Resource Data for Solar Energy Applications: Second Edition. doi:10.18777/ieashc-task46-2015-0001

Seyedmahmoudian, M., Mekhilef, S., Rahmani, R., Yusof, R., Renani, E., 2013. Analytical Modeling of Partially Shaded Photovoltaic Systems. Energies 6, 128–144. doi:10.3390/en6010128

Singh, R., Banerjee, R., 2015. Estimation of rooftop solar photovoltaic potential of a city. Solar Energy 115, 589–602. doi:10.1016/j.solener.2015.03.016

Stein, J.S., Farnung, B., 2017. PV Performance Modeling Methods and Practices Results from the 4th PV Performance Modeling Collaborative Workshop. IEA PVPS Task 13, Subtask 2 Report IEA-PVPS T13-06:2017.

Urraca, R., Martinez-De-Pison, E., Sanz-Garcia, A., Antonanzas, J., Antonanzas-Torres, F., 2017. Estimation methods for global solar radiation: Case study evaluation of five different approaches in central Spain. doi:10.1016/j.rser.2016.11.222

Verso, A., Martin, A., Amador, J., Dominguez, J., 2015. GIS-based method to evaluate the photovoltaic potential in the urban environments: The particular case of Miraflores de la Sierra. Solar Energy 117, 236–245. doi:10.1016/j.solener.2015.04.018

Walch, A., Castello, R., Mohajeri, N., Scartezzini, J.L., 2020. Big data mining for the estimation of hourly rooftop photovoltaic potential and its uncertainty. Applied Energy 262, 114404. doi:10.1016/j.apenergy.2019.114404

Yang, D., 2016. Solar radiation on inclined surfaces: Corrections and benchmarks. Solar Energy. doi:10.1016/j.solener.2016.06.062

Yang, D., 2018. A correct validation of the National Solar Radiation Data Base (NSRDB). Renewable and Sustainable Energy Reviews 97, 152–155. doi:10.1016/J.RSER.2018.08.023

Yang, D., Bright, J.M., 2020. Worldwide validation of 8 satellite-derived and reanalysis solar radiation products: A preliminary evaluation and overall metrics for hourly data over 27 years. Solar Energy. doi:10.1016/j.solener.2020.04.016